Journal of Network Intelligence
Taiwan Ubiquitous Information
 ISSN 2414-8105
Volume **10**, Number **4**, November **2025**

Study on the Control Strategy of Tracking Wind Power Scheduled Output by Energy Storage System

Yang Zhang*

College of Electrical Engineering
North China University of Water Resources and Electric Power
Zhengzhou 450045, P. R. China
zhangyangbeifang@163.com

Dong Kang

College of Electrical Engineering
North China University of Water Resources and Electric Power
Zhengzhou 450045, P. R. China
19723719981@163.com

Jose Lin

College of Science and Technology
Adamson University
Ermita 1000, Manila, Philippines
vu4260@163.com

*Corresponding author: Yang Zhang
Received August 8, 2024, revised February 11, 2025, accepted August 3, 2025.

Abstract. *Energy storage system, with its fast response capability and achieving energy transfer in time and space, provides a feasible solution for broad-scale assimilation of wind power into the electrical network. Nevertheless, the energy storage system's capacity and its ability to charge and discharge are the constraints on its output capability. Additionally, the longevity and the number of cycles it can undergo for charging and discharging are restricted, so setting up a reasonable energy storage control strategy is the key to elevate the system's operational proficiency to consume wind power. Therefore, an energy storage overrun optimisation control strategy with the Dung Beetle Optimizer (DBO) algorithm is proposed. The strategy model introduces variable penalty coefficients, takes into account the energy storage tracking wind power plan deviation and storage charge state, establishes an objective function, and the objective function weight coefficients are adaptively adjusted using a fuzzy controller. In addition, an energy storage overrun optimisation control strategy based on Convolutional Neural Network (CNN) is proposed. The loss function in CNN is used as the adaptation function of DBO algorithm, which achieves the optimisation search of CNN adaptive weights and thresholds, speeds up the iteration speed of the model, and improves the generalisation ability of the model. The outcomes of the simulation demonstrate that the CNN energy storage optimisation control strategy can get rid of the dependence on the energy storage output data of other time periods, and quickly give the energy storage output command of the time period. The simulated scenario confirms the practicality and advantageous nature of the suggested approach.*
Keywords: combined wind storage system; dung beetle optimisation algorithm; energy storage control strategy; convolutional neural network

1. **Introduction.** Wind power and energy storage technology are increasingly closely linked. In recent years, energy storage has assumed a pivotal function in participating in wind power frequency regulation, wind power levelling, and tracking the planned output, showing that energy storage solutions have emerged as a crucial component within renewable energy generation [1, 2]. The energy storage apparatus inherently has limitations regarding its power capabilities and storage capacity. When its power or electricity reaches the maximum or minimum thresholds, the corresponding charging/discharging action cannot continue, thus losing the ability to regulate and causing wind power to deviate from the dispatch plan. Therefore, when tracking the planned wind power output, we should not only minimize the tracking deviation to meet grid requirements, but also account for energy throughput and the regulation ability of the storage system, and formulate a suitable control strategy to avoid the above situation [3, 4].

Stage of Charge (SOC) [5, 6] is an important indicator reflecting the current health status and regulation capability of energy storage. Maintaining an appropriate SOC extends service life, whereas excessive charging or discharging diminishes overall health and future regulation capability. If natural wind output is directly connected to the grid and only the tracking deviation is considered, frequent charge/discharge mode switching may occur, which is not conducive to longevity [7]. Consequently, relying only on ultra–short-term predicted power and current storage output cannot guarantee that future energy accumulation satisfies requirements. A global control strategy for storage power intake and release, while guaranteeing current and future tracking of the planned wind+storage output, is thus of theoretical and practical importance for stable grid integration of wind power.

1.1. **Related work.** With continued research, real-time control strategies for optimal storage output have improved. In wind–storage joint operation, the control strategy must consider not only plan-tracking but also storage capacity [8], power [9], charge state [10], and depth of charge/discharge [11]. In immediate control systems, the deviation between measured and planned (or forecasted) wind output is computed first; wind signals are then decomposed via PI regulation, wavelet packet decomposition, empirical mode decomposition, etc., and the deviation is compensated by controlling storage output. With advances in AI, ML/DL methods are increasingly used: Rodríguez *et al.* [12] designed an integrated ML model for short-term PV interval prediction with fast-correlation feature filtering; Mishra *et al.* [13] proposed a parallel deep model with adaptive weighting combining Attention-Seq2Seq and Transformer; Liu *et al.* [14] combined RF, rough set theory, and DL for short-term load forecasting; Tian [15] used EMD and LMD for joint wind-speed prediction and error correction; Li *et al.* [**?**] built a digital-twin framework using BPNN and a CNN–LSTM–Attention model (with SOC) to analyse and predict Li-ion battery degradation.

1.2. **Motivation and contribution.** To bolster the energy-retention capability of the wind–storage system for tracking the planned wind output, we propose a CNN-based over-advanced optimal control strategy for storage charging/discharging. The main contributions are:

1. **DBO-based overrun optimisation control.** We construct an objective function that jointly considers plan-tracking fluctuation and SOC, introduce variable penalty coefficients, and dynamically adjust them with a fuzzy controller using the Dung Beetle Optimizer (DBO).
2. **CNN-based storage control.** To overcome the time cost and multi–horizon dependence of DBO, we use DBO-derived optimal commands (per time step) together

with wind data as training samples for an improved CNN that outputs storage commands rapidly without relying on other-period storage outputs.

2. Modelling of integrated wind–energy and energy storage systems.

2.1. Wind power system modelling.

We mathematically model the wind turbine, the energy storage system, and the combined wind–storage operation. The wind turbine model includes: a wind turbine aerodynamic model [16], a drive-train model [17], a dynamic model of the Doubly-Fed Induction Generator (DFIG) [18], and a converter model [19].

The DFIG is widely used in modern wind generation due to efficient operation across wind speeds, variable-speed capability, and grid adaptability. Its variable-speed operation enables higher energy-conversion efficiency than fixed-speed machines [20]. Moreover, DFIGs can provide adjustable output and regulate reactive power via the converter. The system comprises the turbine, drive train, generator, and back-to-back converter, which together achieve efficient conversion of wind energy to electrical energy.

2.1.1. *Wind turbine model.* The wind turbine is an important part of the DFIG, the airflow flows through the blades thus driving the blades to rotate and convert the wind energy into mechanical energy, the mechanical power of the wind turbine can be obtained from aerodynamics as shown below:

$$P_w = 0.5\, C_p(\lambda, \beta)\, \pi R^2 \rho V_w^3 \tag{1}$$

where P_w is the power of motor; C_p is energy use coefficient, is related to the tip of the blade speed ratio λ (blade tip of the rotational linear velocity and wind speed ratio) and blade pitch angle β (in engineering practice, C_p is generally 0.2–0.5, the theoretical maximum of 0.593); R for the radius of the blades; ρ for the density of the air (kg/m^3); V_w for the wind speed of the wind farm.

2.1.2. *Drive train modelling.* The transmission serves a crucial function within a wind energy framework and is responsible for efficiently converting the mechanical energy captured by the wind turbine and transferring it to the generator to produce electrical energy. Gearboxes are frequently employed within the drive train to transform the wind turbine's torque motion into the torque output necessary for the generator. The transformation is vital for augmenting the performance and dependability of the wind energy framework. In order to reduce energy losses and simplify maintenance, many modern wind turbines have adopted direct-drive technology, i.e., a gearbox-less design [21, 22], where the wind turbine is directly connected to the generator. Regardless of whether a traditional gearbox or direct-drive technology is used, the design of the drive train will directly determine the operational efficiency and cost-effectiveness of the wind turbine. The transmission system generally contains the drive shaft, variable speed gearbox and generator rotor. The model is generally simplified and analysed using the equivalent mass method, which is divided into single mass block model and double mass block model. The DFIG transmission system model is selected as a double mass block model, i.e., the drive shaft and gearbox are regarded as the first mass block, and the generator rotor is regarded as the second mass block, and its equivalent transfer model can be shown as follows:

$$\begin{cases} p\omega_r = \dfrac{1}{2H_t}[T_m - K_s\theta_s - D(\omega_r - \omega_e)] \\ p\omega_e = \dfrac{1}{2H_g}[K_s\theta_s + D(\omega_r - \omega_e) - T_e] \\ p\theta_s = \omega_r - \omega_e \end{cases} \tag{2}$$

2.1.3. *DFIG dynamic models.* There are two general types of DFIG dynamic models [23], i.e., the space vector model and the d–q model via coordinate transformation. In this paper, the d–q model is used as the dynamic model of DFIG, and its voltage equation is shown below:

$$\begin{bmatrix} u_{sd} \\ u_{sq} \\ u_{rd} \\ u_{rq} \end{bmatrix} = \begin{bmatrix} R_s & 0 & 0 & 0 \\ 0 & R_s & 0 & 0 \\ 0 & 0 & R_r & 0 \\ 0 & 0 & 0 & R_r \end{bmatrix} \begin{bmatrix} i_{sd} \\ i_{sq} \\ i_{rd} \\ i_{rq} \end{bmatrix} + \begin{bmatrix} p & \omega_s & 0 & 0 \\ -\omega_s & p & 0 & 0 \\ 0 & 0 & p & \omega_r - \omega_s \\ 0 & 0 & \omega_s - \omega_r & p \end{bmatrix} \begin{bmatrix} \psi_{sd} \\ \psi_{sq} \\ \psi_{rd} \\ \psi_{rq} \end{bmatrix} \tag{3}$$

where p is the differential operator; R_s is the equivalent stator resistance; R_r is the equivalent rotor resistance; i_{sd}, i_{sq}, i_{rd}, and i_{rq} denote the current components of stator current and rotor current on d-axis and q-axis, respectively; ω_s is the stator angular velocity; ω_r is the rotor angular velocity; ψ_{sd}, ψ_{sq}, ψ_{rd}, and ψ_{rq} denote the magnetic chain components of stator and rotor magnetic chains on d-axis and q-axis, respectively.

The magnetic chain equation is shown below:

$$\begin{bmatrix} \psi_{sd} \\ \psi_{sq} \\ \psi_{rd} \\ \psi_{rq} \end{bmatrix} = \begin{bmatrix} L_s & 0 & L_m & 0 \\ 0 & L_s & 0 & L_m \\ L_m & 0 & L_r & 0 \\ 0 & L_m & 0 & L_r \end{bmatrix} \begin{bmatrix} i_{sd} \\ i_{sq} \\ i_{rd} \\ i_{rq} \end{bmatrix} \tag{4}$$

The power equation is shown below:

$$\begin{bmatrix} P_s \\ Q_s \\ P_r \\ Q_r \end{bmatrix} = \begin{bmatrix} u_{sd} & u_{sq} & 0 & 0 \\ u_{sq} & -u_{sd} & 0 & 0 \\ 0 & 0 & u_{rd} & u_{rq} \\ 0 & 0 & u_{rq} & -u_{rd} \end{bmatrix} \begin{bmatrix} i_{sd} \\ i_{sq} \\ i_{rd} \\ i_{rq} \end{bmatrix} \tag{5}$$

where P_s and P_r are the active electrical energy delivered to the grid originating from both the stator and rotor components, respectively; Q_s and Q_r the grid receives reactive power contributions separately from both the stator and rotor aspects.

The electromagnetic torque equation is shown below:

$$T_e = \frac{3pL_m}{2L_r}\left[\psi_{sd}\, i_{sq} - \psi_{sq}\, i_{sd}\right] \tag{6}$$

2.1.4. *Converter model.* The converter of DFIG contains three types of converters. The control objective of the rotor-side converter is to efficiently capture the wind energy for maximum power output under specific wind speed conditions so that the rotor can be operated at an optimal speed [24]. Also, this control objective includes the elimination of reactive current from the rotor side converter output to maximise the utilisation of its capacity. By controlling the rotor current magnitude, precise regulation of the stator output power and reactive power can be achieved, thereby achieving an efficient and stable functioning of the electrical grid. In this paper, the rotor side converter uses stator voltage directional control so that the direction of the stator voltage vector is in the same direction as the d-axis, then the rotor current equation is shown below:

$$\begin{cases} i_{rd} = -\dfrac{L_s}{L_m}\dfrac{1}{u_{sd}}\, P_s, \\ i_{rq} = \dfrac{L_s}{L_m}\dfrac{1}{u_{sd}}\, Q_s \; - \; \dfrac{u_{sd}}{\omega_s L_m}. \end{cases} \tag{7}$$

With this design of feed-forward current control circuit, the rotor voltage equation is shown below:

$$\begin{cases} u_{rd} = R_r i_{rd} + \sigma L_r \dfrac{di_{rd}}{dt} - \omega_{\text{slip}} \sigma L_r i_{rq}, \\ u_{rq} = R_r i_{rq} + \sigma L_r \dfrac{di_{rq}}{dt} + \omega_{\text{slip}} \sigma L_r i_{rd}, \end{cases} \tag{8}$$

where σ is the control coefficient; $-\omega_{\text{slip}} \sigma L_r i_{rq}$ and $\omega_{\text{slip}} \sigma L_r i_{rd}$ are the voltage feedforward terms.

2.2. **Energy storage system modelling.** This paper focuses on the mathematical modelling of the energy storage's power change, storage charge state and storage charge/discharge power.

The system's operational modes can be categorized into three distinct phases: the charging phase, the discharging phase, and the idle or standby phase. This classification is pivotal for understanding the dynamics of energy storage management. In the process of wind power generation plan execution, the remaining power of the battery energy storage system is an important factor affecting the size of the power levels for charging and discharging processes. The more residual power of the battery energy storage system, the worse its charging power and the stronger its discharge power; conversely, the stronger its charging power and the weaker its discharge power. To streamline the computation of the system's energy intake and output capacities, this study employs a simulation approach that superimposes calculations at each instant. This technique enables a more precise evaluation of the system's energy intake and output capacities, thereby contributing to the enhancement of the operational efficiency and stability within the wind and energy storage hybrid system.

The instantaneous power is contingent upon the residual energy from the preceding moment, the power levels during the prior charging and discharging cycles, the duration of these processes, and the associated charging and discharging efficiencies. This relationship is pivotal for understanding the dynamics of energy storage management and optimizing the system's performance. Its power recurrence formula is shown below:

$$E(t) = (1 - \sigma_{sdr}) E(t-1) + P_c(t) \Delta t \, \eta_c - \frac{P_e(t) \Delta t}{\eta_d} \tag{9}$$

The power $E(t)$ satisfies the must power constraints, which are shown below:

$$E_{\min} \leq E(t) \leq E_{\max} \tag{10}$$

where $E_{\min}$ is the minimum value of power capacity; $E_{\max}$ is the maximum value of power capacity.

The SOC of the energy storage device mirrors the residual energy, defined by the proportion of the instantaneous power at time t to the device's nominal capacity. This parameter is crucial for assessing the system's current energy availability and managing its performance effectively, and its calculation formula is shown below:

$$SOC(t) = \frac{E(t)}{C_{\text{eN}}} \tag{11}$$

where $SOC(t)$ *is the charge state of the power capacity at time* t*;* C_{eN} *is the rated capacity of the power capacity.*

Accurate measurement of the SOC size can timely avoid overcharging or overdischarging of the power capacity, which facilitates the regulation and control of the power capacity, and makes the whole system have a good regulating ability and health. From equation (9), the recurrence relation equation of SOC of power capacity is shown as follows:

$$SOC(t) = (1 - \sigma_{\text{sdr}})\, SOC(t-1) + \eta_c \frac{P_{ec}(t)\,\Delta t_1}{C_{\text{eN}}} + \frac{P_{ef}(t)\,\Delta t_2}{\eta_d\, C_{\text{eN}}} \tag{12}$$

where σ_{sdr} *is the self-discharge rate of the power capacity.*

As to keep the power capacity from overcharging or overdischarging, which can affect the service life of the power capacity, maximum and minimum thresholds are set for the SOC as shown below:

$$SOC_L \le SOC(t) \le SOC_H \tag{13}$$

Secondly, the energy input and output capabilities of the power capacity is not only limited by its own maximum allowable power, but also related to the remaining capacity of the power capacity at the current time, whose constraints are shown below:

$$\begin{cases} \max\left\{ P^1_{\max},\ \dfrac{(1-\sigma_{\text{sdr}})\,E(t-1) - E_{\max}}{\eta_c\,\Delta t} \right\} \le P_e(t), \\ \min\left\{ P^2_{\max},\ \dfrac{\left[(1-\sigma_{\text{sdr}})\,E(t-1) - E_{\min}\right]\eta_d}{\Delta t} \right\} \ge P_e(t). \end{cases} \tag{14}$$

2.3. **Wind storage combined system model.** The hybrid wind-storage system is composed of three primary components: a wind energy conversion segment, an energy management hub, and an energy storage segment. The wind energy conversion segment transforms wind energy into mechanical energy, which is subsequently converted into electrical energy. This segment is comprised of multiple wind turbines, serving as the core power generation units for the integrated wind-storage system. The energy management hub gathers real-time data on wind power output and the current status of the energy storage. Utilizing this information, along with the operational status of the wind farm and the power capacity, the hub formulates an active power control strategy for the storage. This strategy is then communicated to the power capacity in the form of dispatch commands. The energy storage segment is made up of numerous energy storage batteries. These batteries are charged and discharged following the dispatch directives to ensure that the wind farm's total output aligns with the grid's dispatch plan. This process also considers the health and regulatory capacity of the power capacity to maintain optimal performance and longevity.

Neglecting the losses between the various parts of the system, the grid-connected power equation of the wind power capacity and the recurrence formula of the energy storage capacity can be obtained as follows, respectively:

$$P_{\text{grid}}(t) = P_w(t) + P_e(t) \tag{15}$$

$$C_e(t) = C_e(t-1) - \eta\, T\, P^e_s(t-1) \tag{16}$$

where $P_{\text{grid}}(t)$ is the grid-connected power of wind power at the time t; $P_w(t)$ is the actual power of wind power at the time t; $P_e(t)$ is the power at the time t; $C_e(t)$ is the power capacity at the time t; η is the charging/discharging efficiency; T_s is the time interval; and $C_e(t-1)$ is the storage capacity at the time $t-1$;

3. **DBO-based optimal control strategy.**

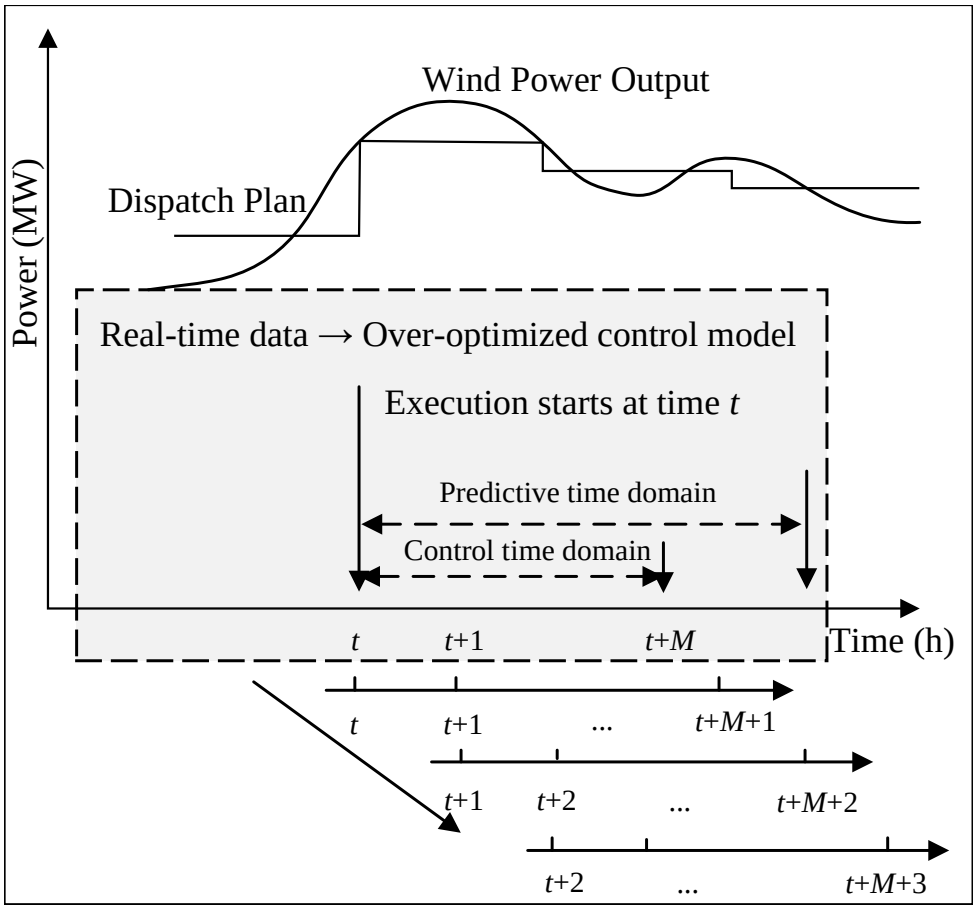

Figure 1. Over-the-horizon optimisation control schematic

3.1. **Over-the-horizon optimal control.** The principle of ahead-of-time optimisation control is shown in Figure 1. The first step of the ahead-of-time optimisation control strategy is to set up a rolling optimisation time window. The length of this window is limited to the time scale of the ultrashort-term prediction of power data within a day. The length of the optimisation window is usually chosen to be shorter than the duration of the exceedingly short-term predicted power, taking into account that the precision of the exceedingly short-term prediction may decrease over time. Next, the required data points for the window period are collected. Ultimately, the data from these moments are input into the objective function of the intraday efficient allocation to solve for the optimal energy storage system output for that time period.

By iterating forward through the over-optimised control model, the future $t+i$ time state vector and output vector are obtained as shown below:

$$\begin{cases} \boldsymbol{x}(t) = \left[\, \boldsymbol{x}(t+1\,|\,t),\, \boldsymbol{x}(t+2\,|\,t),\, \ldots,\, \boldsymbol{x}(t+M\,|\,t) \,\right]^T, \\ \boldsymbol{y}(t) = \left[\, \boldsymbol{y}(t+1\,|\,t),\, \boldsymbol{y}(t+2\,|\,t),\, \ldots,\, \boldsymbol{y}(t+M\,|\,t) \,\right]^T. \end{cases} \tag{17}$$

where $\boldsymbol{x}(t+i\,|\,t)$, $\boldsymbol{y}(t+i\,|\,t)$ $(i=1,2,3,\ldots,M)$ are the state vectors and output vectors at time t predicting the time $t+i$, and M is the step size of the control time domain.

At the time $t+i$, the state vector $x(t+i\,|\,t+i-1)$ obtained from the previous iteration is updated to carry out the over-rolling optimisation, and the optimal control sequence of energy storage for each time period is obtained as shown below:

$$\Delta u(t+i) = \left[\, \Delta u(t+1),\, \Delta u(t+2),\, \ldots,\, \Delta u(t+M) \,\right]^{\top} \tag{18}$$

3.2. **Objective function.** The current research of energy storage optimisation control model mostly adopts the minimum amount of tracking deviation, the minimum comprehensive cost of wind–storage joint system, and the optimal storage charge state as the objective function. The wind power of these methods is characterised by large fluctuations and rapid changes, and at the same time, due to the limited energy storage capacity, it is easy to lead to a situation where the energy storage output cannot meet the requirements in time. In the tracking wind power plan, we aim not only to make the energy storage track the plan while meeting grid constraints, but also to maintain a good charging/discharging scheduling ability. In this paper, we comprehensively consider tracking wind-power plan deviation, energy-storage charge state, and target-value deviation to construct the objective function.

(1) Minimal tracking wind-plan deviations f_1.

$$\beta = \frac{P_{\text{grid}}(t+i) - P_{\text{alm}}(t+i)}{\alpha\, P^{\text{plan}}} \tag{19}$$

$$\min f_1 = \sum_{i=1}^{M} \left(\frac{2}{1 + e^{\,b(\beta - c)}} \left(P_{\text{grid}}(t+i) - P_{\text{alm}}(t+i) \right)^2 \right) \tag{20}$$

(2) Minimal target-value deviation of the charge state f_2.

$$\min f_2 = \sum_{i=1}^{M} \left(\frac{2}{1 + e^{\,d\left((\text{SOC}(t+i) - \text{SOC}_{\text{aim}}) - e \right)}} \left(\text{SOC}(t+i) - \text{SOC}_{\text{aim}} \right)^2 \right) \tag{21}$$

$$\text{SOC}(t+i) = \text{SOC}(t) + \eta \frac{P_e(t)\, T_s}{C_{eN}} \tag{22}$$

where $\text{SOC}(t+i)$ is the predicted charge state of the energy storage system at the time $t+i$; SOC_{aim} is the target value of the charge state of the energy storage, the target value is generally taken as half of the rated capacity of the energy storage.

In the realm of control temporal dynamics, the aspiration is for the energy storage to exhibit robust tracking capabilities in alignment with the projected output and to possess commendable regulatory proficiency. Considering the above factors, each part is weighted to obtain the objective function that tracks the deviation of wind power plan and minimises the deviation of storage SOC from the target value:

$$\min J = a\, f_1 + (1 - a)\, f_2 \tag{23}$$

where a is the weight coefficient; its value is obtained from the fuzzy controller.

3.3. **Adaptive control of weighting factor a.** The energy storage system output size $P_e(t+i)$ is affected by the size of the weighting coefficient a value. The larger the a value is, the better the tracking effect of energy storage is, but the more the state of energy storage charge deviates from the target value, and the over-limit may occur; the smaller the a value is, the closer the residual capacity of energy storage is to the target value, but the worse the tracking effect is. Reasonable setting of a value size can optimise the system tracking effect and energy storage charge state. Therefore, in this paper, a double fuzzy controller is used to determine the size of the a value.

The deviation $D(t+i)$ of the ultra-short-term predicted power of wind power from the generation plan at the time $t+i$ can be obtained from Equation (24).

$$D(t+i) = P_{aim}(t+i) - P_{plan}(t+i) \tag{24}$$

Design a two-input single-output fuzzy controller. Firstly, input one is defined as the state of charge $SOC(t)$ of the energy storage system at time t. The fuzzy subset is [VS, S, M, B, VB], which represents "very small", "small", "medium", "large", "very

Table 1. Reasoning table of controller 1

a	$P_e(t)$				
	NB	NM	M	PM	PB
$SOC(t)$ VS	M	B	PB	JB	ZB
$SOC(t)$ S	B	PB	ZB	PB	JB
$SOC(t)$ M	JB	ZB	ZB	ZB	JB
$SOC(t)$ B	JB	PB	ZB	PB	B
$SOC(t)$ VB	ZB	JB	PB	B	M

Table 2. Reasoning table of controller 2

a	$P_e(t)$				
	NB	NM	M	PM	PB
$SOC(t)$ VS	VB	PB	M	M	ZB
$SOC(t)$ S	PB	M	PS	M	JB
$SOC(t)$ M	VS	VS	PS	VS	JB
$SOC(t)$ B	M	M	PB	M	B
$SOC(t)$ VB	M	PB	VB	VB	M

large", and the range of action is [0.2,0.8]. Secondly, input two is the energy storage system output value $P_e(t)$ at time t. The fuzzy subsets are [NB, NM, M, PM, PB], which are represented in order as "negative large", "negative medium", "Medium", "Positive Medium", "Positive Large", and the range of action is $[-P_e, P_e]$, and P_e is charging and discharging power limits of the energy storage system. Then, the output is defined as the weight coefficient a, and the fuzzy subsets are [M, B, PB, JB, ZB], which in turn denote "medium", "large", "large "very large", "maximum", and the range is [0.5,1]. The fuzzy reasoning table of two controllers is shown in Table 1 and Table 2 respectively.

In this paper, the weighted average method is used to perform real-time defuzzification of the fuzzy control method designed in this paper, so as to derive the size of the weight coefficients a value corresponding to the $t + i$ time.

4. **CNN-based real-time control strategy for energy storage.** This paper combines the DBO algorithm with a CNN. The DBO algorithm draws its conceptual framework from the natural actions of dung beetles, encapsulating their activities such as rolling balls, engaging in dances, searching for food, seizing opportunities, and reproducing. This technique integrates these behaviors into the hyperparameters of the CNN model and employs the CNN's loss function as the fitness measure for the DBO. This integration facilitates the construction of the DBO-CNN predictive model, leveraging the natural strategies of dung beetles to optimize the performance of the CNN. The hyperparameters include the weights and thresholds of the CNN. In the realm of hyperparameter optimization, the position of each dung beetle symbolizes a unique combination of hyperparameter settings. This representation is instrumental in navigating the hyperparameter space to identify the most effective configuration for the model. Meanwhile, the initial position of the dung beetle is set randomly to ensure that the whole search space can be searched completely. The CNN adopts the mean-square error. The updating process of dung beetle position makes the value of Equation (25) minimum.

$$\text{loss} = \frac{\sum_{i=1}^{n} (y - y')^2}{n} \tag{25}$$

where n is the number of samples; y is the output value of the model; y' is the actual value of the sample.

Within the framework of the DBO algorithm, the dung beetle explores the solution space using its ball-rolling behaviour. When encountering obstacles, the dung beetle's "dancing" behaviour is used to relocate, which is modelled in the algorithm as an update mechanism when the solution falls into a local optimum, in order to go beyond the local optimum in search of a globally optimal solution. In the algorithm, the natural behaviour of female dung beetles laying eggs at a specific location is modelled as a breeding area in the solution space for generating new solutions, which is dynamically adjusted according to the algorithmic progress in order to satisfy the need for both wide-area exploration and locally fine-tuned search. Meanwhile, as young dung beetles grow up, they search for food and head towards easily recognisable food source regions, a behaviour that corresponds in the algorithm to updating the position of young dung beetles within preferred food regions. In addition, the "stealing" of dung balls among dung beetles is modelled in the algorithm as a way to increase the probability of finding the globally optimal solution by generating new solutions close to the optimal solution.

1. Training set generation, where a certain percentage of the provided samples are chosen at random for the training dataset.
2. Initialise the weights and thresholds of the CNN, set the number of dung beetle populations n, the dimension of the variable to be optimised to be d, initialise the number of dung beetle populations, set upper and lower bounds on the initial values, and the maximum number of iterations;
3. The weights and thresholds of the CNN are used as hyperparameters of the DBO algorithm, which are reflected by the location information of the dung beetle, and the CNN forward propagation calculation is performed to compute the value of the loss function, i.e., the size of the DBO algorithm's fitness.
4. Calculate the fitness of each individual dung beetle to obtain the position information of the dung beetle with the smallest fitness value at this time, which is recorded as the historical optimal position.
5. Update the dung beetle position by the behaviour of each type of dung beetle, calculate the value of adaptation after updating, and obtain the dung beetle position information corresponding to the minimum adaptation after updating the position information.
6. Compare the current dung beetle optimal position information and the historical dung beetle optimal position information to get the global dung beetle optimal position information.
7. Assess if the stopping criterion for the iterative process has been met. If it meets, then terminate the iteration and output the global optimal position information, if not, then return to step (3) and repeat the execution until the termination condition is met.
8. The hyperparameters represented by the global optimal dung beetle location information, i.e., the CNN weights and thresholds, are taken and used at this point in time to predict the output of the power storage apparatus using the CNN model.

5. **Example analyses.**

5.1. **Data collection.** The training samples are the actual operation data of a real wind farm for three months (July, August, and September) in the previous section, i.e., the known power generation plan for each time period, the actual wind power, the lower limit of the planned output, the upper limit of the planned output, the SOC of the storage,

and the storage output calculated by the storage overrun optimal control strategy with DBO algorithm. The sampling frequency is 5 min, a total of 26,496 data sets.

5.2. **Network parameters.** In this paper, the feature volume is not of high dimensionality and the architecture of the CNN is not set up with a pooling layer. The first fully connected layer is set with 120 neurons, while the last fully connected layer is used to generate the predicted value of the stored energy output. In the training phase of the network, batch processing is used in groups of 24 samples. During the training process, a batch processing strategy of 24 samples per batch is used. The input feature quantities for a time period t are the ultra-short-term forecast power, wind power, planned output, upper limit of planned output, lower limit of planned output, and storage SOC for that time period; and the output feature quantity is the storage output for that time period. That is, the real-time control strategy tracking wind power planned output is carried out by this method.

5.3. **Evaluation indicators.** To demonstrate the viability and superiority of the control methodologies introduced in this manuscript, the subsequent trio of strategies have been established for a comparative evaluation.
Strategy 1: Support Vector Machine (SVM).
Strategy 2: CNN.
Strategy 3: The proposed DBO–CNN.
To evaluate the merits of the control strategy, RMSE, MAE and MAXE were used to assess the prediction performance of the model:

$$\mathrm{RMSE} = \sqrt{\frac{1}{n}\sum_{i=1}^{n}(P_{Mi} - P_{Pi})^2} \tag{26}$$

$$\mathrm{MAE} = \frac{1}{n}\sum_{i=1}^{n}|P_{Mi} - P_{Pi}| \tag{27}$$

$$\mathrm{MAXE} = \max_{i}|P_{Mi} - P_{Pi}| \tag{28}$$

where n is the number of predicted samples; P_{Mi} is the actual value of the energy storage capacity of the i-th sample; and P_{Pi} is the predicted value of the energy storage capacity of the i-th sample.

5.4. **Analysis of results.** In this paper, three machine learning methods, namely DBO-CNN, CNN and SVM, are used to train the samples respectively. CNN adopts Adam to update the weight parameters, regularisation and dropout methods to avoid overfitting, the learning rate is set to 0.001, and the number of layers, the number of neurons and the excitation function are all the same as that of DBO-CNN. SVM adopts the radial basis kernel function, with the penalty coefficient of 4, and the radial basis function parameter is 0.8.

After the training of the DBO-CNN method is completed, the comparison of the real value of the storage output and the predicted value of the storage output in the test set is shown in Figure 2. The results of the evaluation indexes of different models in the test set are shown in Table 3.

The horizontal coordinate in Figure 2 indicates the number of samples and the vertical coordinate indicates the magnitude of the predicted energy storage output. The DBO-CNN prediction model proposed in this paper is more consistent with the predicted energy storage output value and the actual energy storage output value in the test set of 2,650 samples after 23,846 times of training samples training.

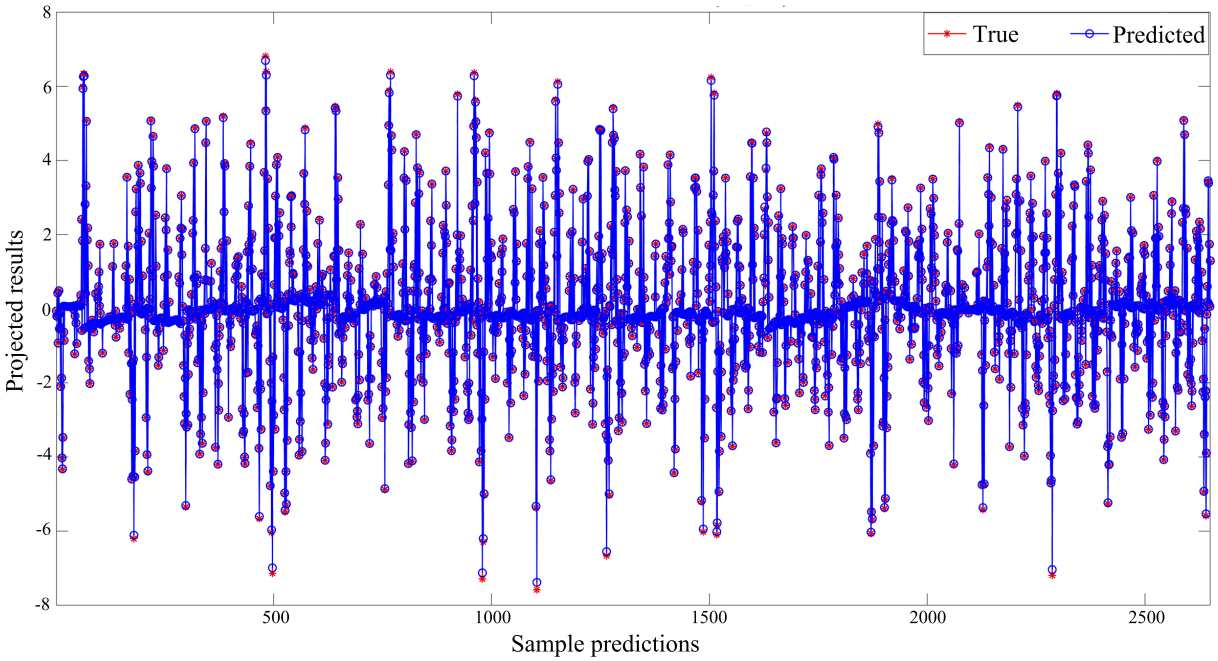

Figure 2. Graph comparing the true and predicted values of the DBO-CNN test set

Table 3. Comparative table of evaluation indicators

Control strategy	**Set**	**RMSE (MW)**	**MAE (MW)**	**MAXE (MW)**
DBO-CNN	Training set	0.017066	0.009054	0.36323
	Test set	0.014709	0.00842	0.19959
CNN	Training set	0.05974	0.047379	0.32881
	Test set	0.057661	0.045644	0.24174
SVM	Training set	0.072618	0.052713	0.82515
	Test set	0.071335	0.052749	0.55866

As can be seen from Table 3, in the test set performance of the samples, the root mean square deviation *RMSE* of the SVM model prediction is 0.071335 MW, which is the largest value among the three prediction models selected in this paper, indicating that the SVM model prediction accuracy is low and the model prediction is not good; the original CNN model is used to predict the energy storage output than the *RMSE* of the SVM model prediction is reduced with a size of 0.057661 MW, a reduction of 0.013674 MW, indicating that the prediction accuracy of the original CNN model is improved over SVM; and the DBO-CNN model proposed in this paper has a substantial reduction in the root mean square deviation compared to the original CNN model and the SVM model, the magnitude of which is 0.014709 MW. In terms of the mean absolute deviation *MAE*, the SVM model predicts an average absolute deviation of 0.014709 MW. The mean absolute deviation size is 0.052749 MW, which is the largest value among the three models, and the mean absolute deviation predicted by the CNN model for energy storage output is reduced by 0.007105 MW compared to that predicted by the SVM model, and the mean absolute deviation size predicted by the DBO-CNN model is only 0.00842 MW, which indicates that the prediction accuracy of its model is the highest. the SVM model, SVM model, the original CNN model and the DBO-CNN model have an average relative deviation of 0.01119 MW, 0.001864 MW and 0.000666 MW, respectively, and the average relative

deviations of the three models are positive, indicating that the predicted output values of the three models for energy storage are all higher than the actual values of the energy storage outputs, and that the DBO-CNN model has the smallest predicted average relative deviation and the highest accuracy. The maximum prediction deviation of SVM model is 0.55866 MW, which is the largest value among the three prediction models, followed by CNN prediction model with 0.24174 MW, and the maximum prediction deviation of DBO-CNN model is 0.19959 MW, which is the smallest value among the three prediction models, indicating that the stability of the DBO-CNN prediction model is the best. In summary, the model prediction effect of the DBO-CNN energy storage output prediction model is better than that of CNN model and SVM model in both the training set and the test set, and the stability of its model is good, the accuracy is high, the prediction deviation is small, and the performance of each evaluation index is the best.

6. **Conclusion.** Aiming at the problem of energy storage tracking wind power plan output, an energy storage overrun optimisation control strategy based on the DBO is proposed, which can effectively reduce the deviation of the joint wind-storage grid tracking wind power scheduling plan while taking into account the charge state. While satisfying the current output plan, it takes into account the regulation capability in the future time, optimises the health, extends the applicable life, and improves the benefits of the combined wind and storage system. In addition, a CNN-based energy storage overrun optimisation control strategy is proposed. The loss function in CNN is used as the adaptation function of DBO algorithm, which achieves the optimisation of CNN adaptive weights and thresholds, speeds up the iteration speed of the model, and improves the generalisation ability of the model, and the simulation results show that the CNN energy storage optimisation control strategy can get rid of the dependence on the energy storage output data of other time periods, and quickly give the output instruction of the energy storage of the time period, and improve the control speed.

REFERENCES

[1] J.-H. Zhu, W.-X. Pan, and X. Li, "Energy storage scheduling design on friendly grid wind power," *Sustainable Energy Technologies and Assessments*, vol. 25, pp. 111–118, 2018.

[2] M. Cao, Q. Xu, X. Qin, and J. Cai, "Battery energy storage sizing based on a model predictive control strategy with operational constraints to smooth the wind power," *International Journal of Electrical Power & Energy Systems*, vol. 115, p. 105471, 2020.

[3] J.-H. Zhu, R. Xu, J. Gu, X. Zhang, and C. Sun, "Wind/Storage Power Scheduling Based on Time–Sequence Rolling Optimization," *Arabian Journal for Science and Engineering*, vol. 48, no. 5, pp. 6219–6236, 2022.

[4] Q. Zhang, X. Chen, G. Li, J. Feng, and A. Yang, "Model Predictive Control Method of Multi-Energy Flow System Considering Wind Power Consumption," *IEEE Access*, vol. 11, pp. 86697–86710, 2023.

[5] Y. Yu, D. Chen, B. Wang, Y. Wu, W. Lu, and Z. Mi, "Control scheme to extend lifetime of BESS for assisting wind farm to track power generation plan based on wind power feature extraction," *IET Power Electronics*, vol. 15, no. 15, pp. 1629–1651, 2022.

[6] X. Han, D. Liang, and H. Wang, "An optimization scheduling method of electric vehicle virtual energy storage to track planned output based on multiobjective optimization," *International Journal of Energy Research*, vol. 44, no. 11, pp. 8492–8512, 2020.

[7] B. Li, X. Mo, and B. Chen, "Direct Control Strategy of Real-Time Tracking Power Generation Plan for Wind Power and Battery Energy Storage Combined System," *IEEE Access*, vol. 7, pp. 147169–147178, 2019.

[8] B. Wang, G. Cai, and D. Yang, "Dispatching of a Wind Farm Incorporated With Dual-Battery Energy Storage System Using Model Predictive Control," *IEEE Access*, vol. 8, pp. 144442–144452, 2020.

[9] S. Zhao, L. Zhou, Q. Zhang, S. Dang, H. Yu, G. Zhang, R. Guo, and W. Zhao, "Research on electric vehicle-supercapacitor hybrid system participates in the application of tracking PV project output," *Energy Science & Engineering*, vol. 10, no. 1, pp. 120–131, 2021.

[10] S. Kumar, K. K. Mandal, and N. Chakraborty, "Optimal placement of different types of DG units considering various load models using novel multiobjective quasi-oppositional grey wolf optimizer," *Soft Computing*, vol. 25, no. 6, pp. 4845–4864, 2021.

[11] M.-T. Kuo, "Application of the Artificial Bee Colony Algorithm to Scheduling Strategies for Energy-Storage Systems of a Microgrid With Self-Healing Functions," *IEEE Transactions on Industry Applications*, vol. 57, no. 3, pp. 2156–2167, 2021.

[12] F. Rodríguez, A. Galarza, J. C. Vasquez, and J. M. Guerrero, "Using deep learning and meteorological parameters to forecast the photovoltaic generators intra-hour output power interval for smart grid control," *Energy*, vol. 239, p. 122116, 2022.

[13] M. Mishra, P. B. Dash, J. Nayak, B. Naik, and S. K. Swain, "Deep learning and wavelet transform integrated approach for short-term solar PV power prediction," *Measurement*, vol. 166, p. 108250, 2020.

[14] F. Liu, T. Dong, T. Hou, and Y. Liu, "A hybrid short-term load forecasting model based on improved fuzzy c-means clustering, random forest and deep neural networks," *IEEE Access*, vol. 9, pp. 59754–59765, 2021.

[15] Z. Tian, "Short-term wind speed prediction based on LMD and improved FA optimized combined kernel function LSSVM," *Engineering Applications of Artificial Intelligence*, vol. 91, p. 103573, 2020.

[16] W. Li, Y. Li, A. Garg, and L. Gao, "Enhancing real-time degradation prediction of lithium-ion battery: A digital twin framework with CNN-LSTM-attention model," *Energy*, vol. 286, p. 129681, 2024.

[17] J. Xue and B. Shen, "Dung beetle optimizer: a new meta-heuristic algorithm for global optimization," *The Journal of Supercomputing*, vol. 79, no. 7, pp. 7305–7336, 2022.

[18] J. Mitali, S. Dhinakaran, and A. A. Mohamad, "Energy storage systems: a review," *Energy Storage and Saving*, vol. 1, no. 3, pp. 166–216, 2022.

[19] A. G. Olabi, C. Onumaegbu, T. Wilberforce, M. Ramadan, M. A. Abdelkareem, and A. H. Al–Alami, "Critical review of energy storage systems," *Energy*, vol. 214, p. 118987, 2021.

[20] T.-Y. Wu, H. Li, S. Kumari, and C.-M. Chen, "A Spectral Convolutional Neural Network Model Based on Adaptive Fick's Law for Hyperspectral Image Classification," *Computers, Materials & Continua*, vol. 79, no. 1, pp. 19–46, 2024.

[21] T.-Y. Wu, A. Shao, and J.-S. Pan, "CTOA: Toward a Chaotic-Based Tumbleweed Optimization Algorithm," *Mathematics*, vol. 11, no. 10, p. 2339, 2023.

[22] T.-Y. Wu, H. Li, and S.-C. Chu, "CPPE: An Improved Phasmatodea Population Evolution Algorithm with Chaotic Maps," *Mathematics*, vol. 11, no. 9, p. 1977, 2023.

[23] A. G. Olabi, T. Wilberforce, M. Ramadan, M. A. Abdelkareem, and A. H. Alami, "Compressed air energy storage systems: Components and operating parameters – A review," *Journal of Energy Storage*, vol. 34, p. 102000, 2021.

[24] M. Mahmoud, M. Ramadan, A.-G. Olabi, K. Pullen, and S. Naher, "A review of mechanical energy storage systems combined with wind and solar applications," *Energy Conversion and Management*, vol. 210, p. 112670, 2020.

[25] E. Hossain, H. Faruque, M. Sunny, N. Mohammad, and N. Nawar, "A Comprehensive Review on Energy Storage Systems: Types, Comparison, Current Scenario, Applications, Barriers, and Potential Solutions, Policies, and Future Prospects," *Energies*, vol. 13, no. 14, p. 3651, 2020.

[26] D. Bhatt, C. Patel, H. Talsania, J. Patel, R. Vaghela, S. Pandya, K. Modi, and H. Ghayvat, "CNN Variants for Computer Vision: History, Architecture, Application, Challenges and Future Scope," *Electronics*, vol. 10, no. 20, p. 2470, 2021.